Simultaneous Design and Control of a Semibatch Styrene Polymerization Reactor

Mariano Asteasuain, Adriana Brandolin, Claudia Sarmoria, and Alberto Bandoni*

Planta Piloto de Ingeniería Química (UNS, CONICET), Camino La Carrindanga, km 7, 8000 Bahía Blanca, Argentina

It has been established that the security, flexibility, and dynamic controllability of a process are inherent properties of its design, which also affects process economics. In this context, we employed a previously developed mixed-integer dynamic optimization (MIDO) approach to perform the simultaneous design and control of styrene polymerization reactors. Industrial- and laboratory-size semibatch jacketed reactors were considered. The gPROMS/gOPT package was successfully used to solve the mixed-integer dynamic optimizations. In each case, the geometry, initiator mixture composition, and control system were optimally determined in a single optimization run. We analyzed the effect of using different coolants with and without heat supply on the laboratory-scale reactor design. We also studied the effect of scale-up in the integrated process and control design. Design coincidences and differences were analyzed.

1. Introduction

Polymeric materials are extremely important in industry. They present a great versatility and a high production rate, of nearly 200 million tons each year.[1] Their countless uses range from everyday objects, such as food packaging, to high-tech applications, such as surgery implants.

Polymer flow properties during processing (i.e., viscosity, elasticity) and end-use properties (i.e., density, flow index, impact strength, tensile strength, stiffness, chemical resistance, thermal stability) can be correlated with the polymer molecular structure and morphology.[2,3] In turn, molecular properties depend strongly on the operating conditions under which the polymer is synthesized or modified. Thus, a detailed understanding and control of these processes is fundamental to the efficient production of tailored polymers without significant operating problems.[4] Polymerization processes often present highly exothermic reactions and significant viscosity variations along the reaction path, leading to complex heat transfer and fluid dynamics. As discussed in the review by Ray and Villa,[5] the dynamic behavior of polymerization reactors is highly nonlinear. Control of processes with these characteristics is a challenging task.[6,7] In the particular field of polymerization processes, this has motivated abundant research into the development of accurate mathematical models,[8,9] process optimizations, and efficient control schemes.[10]

Most batch and semibatch polymerization reactors are controlled by preprogrammed recipe implementation and temperature controls that are commonly based on heat balances. Extensive discussions on batch and semibatch polymerization reactor control strategies and the techniques used to calculate them can be found elsewhere.[7,10−13] For example, MacGregor et al.[11] reported the control of molecular properties in bulk free-radical polymerization by means of temperature variations or semicontinuous operation. They achieved this by adding combinations of initiator, monomer, and chain-transfer agents at certain times after the start of the reaction. Crowley and Choi[12] determined an optimal sequence of reactor temperature set points to attain a desired molecular weight distribution for a batch solution free-radical polymerization. In another work,[14] these authors studied a free-radical suspension polymerization in a batch reactor and determined the optimal temperature trajectory and initial initiator concentration so as to minimize the squared difference between the desired and actual tensile strength of the product. As the authors mentioned, what they calculated was an optimal temperature set-point profile, assuming that this set-point sequence could be tracked reasonably well by a real-time controller. Rafizadeh[15] designed a sequential linearization adaptive PI controller to control the temperature of a batch methyl methacrylate (MMA) polymerization reactor. This author used a suitable temperature trajectory taken from the literature, obtaining good temperature control. Yabuki et al.[16] proposed midpoint correction policies to attain the control of a given product quality for industrial semibatch solution and emulsion polymerizations.

Traditionally, operational aspects (optimum operation and control) have been treated sequentially with the system design. That is, first the process is designed to achieve an optimum objective based on a fully specified nominal case. Only after the process or equipment has been designed are operability aspects taken into account. These might include the control system design and the safety, reliability, and flexibility of the design. The sequential approach to these two fundamental problems does not take into account the fact that process safety, stationary-state flexibility, and dynamic controllability are inherent properties of process design, also affecting process economics.[17] The importance of dealing with design and operability simultaneously has been recognized for many years,[18] and in the past 2 decades, there has been increasing interest from both academia and industry in the field.[19] Some works can be found in the literature that attack these two problems with different approaches,[17,19−26] but only Chatzidoukas et

* To whom correspondence should be addressed. Tel.: (54)-2914861700 ext 272. Fax: (54)-2914861600. E-mail: abandoni@plapiqui.edu.ar.

10.1021/ie040021s CCC: $27.50
Published on Web 07/13/2004

al.[26] have focused on a polymerization process, specifically, one in which a fixed reactor for gas-phase ethylene copolymerization is undergoing a specific polymer grade change. They simultaneously designed the optimal trajectories of the process variables and the control system. To the best of our knowledge, no attempt to perform the simultaneous designs of reactor geometry, process, and control system for styrene bulk polymerization has previously been reported in the open literature.

Some of the relevant techniques that have been proposed for the integration of process design and operability include flexibility analysis (based on nonlinear programming and steady-state models), resiliency studies (based on linear multivariable models), and steady-state and dynamic "back-off" analysis (where the actual operating point is chosen by "backing off" from the optimum point that lies at the intersection of constraints). The main disadvantage of most of these methods is that, even though they provide a quantitative measure of the system's controllability and allow for the comparison of different designs on a common basis, they often do not give a precise guide for changes in process and/or control design. Moreover, they are usually based on linear models, and in many cases, it is doubtful whether the conclusions obtained can be extrapolated to the real system.[19] This issue can become particularly relevant for a highly nonlinear process such as a polymerization.

In this work, a different approach is used for the simultaneous design and control of industrial- and laboratory-scale semibatch styrene polymerization processes. It consists of solving a single optimization problem in which both process design variables and control system are optimally determined. At the same time, feasible operation is achieved, where feasibility is defined in terms of product specifications and process constraints. A rigorous model of the process is used[27] that is an extension of a previous model that has been validated against experimental data.[28] It should be noted that the optimization problem requires discrete decisions (selection of the initiators to include in the initiator mixture and selection of the manipulated variables), giving rise to a mixed-integer dynamic optimization problem (MIDO). This is, in general, a very difficult task for which efficient solution methods are currently subject to intensive research. A few works have recently been reported in chemical engineering dealing with MIDO problems, with different solution approaches.[22,23,26,29−32] In this work, the resulting MIDO problem is solved by means of the gPROMS/gOPT v.2.2.3 package (Process Systems Enterprise Ltd.).

2. Mathematical Model

The process under study is the bulk free-radical polymerization of styrene in semibatch reactors using (possibly) a complex initiator mixture of different peroxides. The reactors have cooling jackets and an optional heat supply. Once the monomer is preheated to the initial reaction temperature (T_0), the initiator mixture is added. Therefore, we consider that the initial reacting medium consists of the monomer and the initiator mixture at T_0. Peroxides can also be added during the course of the reaction. The initiator system is a critically important parameter in free-radical polymerization. Through appropriate initiator selection, it is possible to enhance reactor performance to increase production, achieve certain molecular properties, or improve controllability. Initiators of different functionalities have been used for styrene polymerization. The superiority of bifunctional initiators with respect to monofunctional ones has been demonstrated,[33−42] as they allow high molecular weights and high polymerization rates to be achieved simultaneously. However, some authors have analyzed the possibility of using different mixtures of bifunctional and monofunctional initiators,[39] with promising results.

A previous kinetic scheme describing the bulk polymerization of styrene with an asymmetric bifunctional initiator[27] has been slightly modified to allow for the possibility of using a mixture of mono- and bifunctional initiators under batch or semibatch operation. In addition, heat balances for the reaction mixture and the cooling jacket have been added. The previous model provided a good representation of experimental data.[27] The kinetic steps of the new model are listed in Table 1.

This is a rather complex kinetic mechanism that leads to 10 macromolecular species coexisting in the reaction mixture: macroradicals $R_n^{\bullet}$, $R_n^{\bullet A}$, $R_n^{\bullet B}$, and $R_n^{\bullet\bullet}$; temporary polymers P_n^{A}, P_n^{B}, P_n^{AB}, P_n^{AA}, and P_n^{BB}; and permanent polymer P_n. The molecular properties that we analyze in this work are the number- (M_n) and weight- (M_w) average molecular weights of the overall macromolecular species and the polydispersity index (Pd), which are calculated according to eqs 1−3, respectively

$$M_n = M_{mon}\frac{\sum Y_1^{\gamma} + \sum M_1^{\lambda}}{\sum Y_0^{\gamma} + \sum M_0^{\lambda}} \tag{1}$$

$$M_w = M_{mon}\frac{\sum Y_2^{\gamma} + \sum M_2^{\lambda}}{\sum Y_1^{\gamma} + \sum M_1^{\lambda}} \tag{2}$$

$$Pd = \frac{M_w}{M_n} \tag{3}$$

In these equations, the superscript γ is one of •, •A, •B, and ••; the superscript λ is one of A, B, AB, AA, BB, and permanent polymer (no superscript). M_{mon} is the monomer molecular weight, Y_a^{γ} and M_a^{λ} are the ath-(a = 0, 1, 2) order moments of the macroradical and polymer molecular weight distributions, respectively, which are defined as

$$Y_a^{\gamma} = \sum_{n=1}^{\infty} n^a R_n^{\gamma}$$

$$M_a^{\lambda} = \sum_{n=1}^{\infty} n^a P_n^{\lambda} \tag{4}$$

To calculate these moments, mass balance equations must be set up for all macroradical and polymer species. Then, these equations are transformed to obtain balance equations for Y_a^{γ} and M_a^{λ}. Details about this procedure can be found in Asteasuain et al.[27] The resulting moment balances are presented in Tables 2 and 3. They are solved together with the mass balances for monomer, peroxide initiators, and initiation radicals, presented in Table 4. The rate of change of the reaction mixture volume (V) is also described in this table.

Table 1. Kinetic Mechanism

Peroxide Decomposition

in initiators

$$I_B \xrightarrow{k_{d_B}} R^\bullet + R^{\bullet A}$$

$$I_B \xrightarrow{k_{d_A}} R^\bullet + R^{\bullet B}$$

$$I_{MA} \xrightarrow{k_{d_A}} 2R^\bullet$$

$$I_{MB} \xrightarrow{k_{d_B}} 2R^\bullet$$

in initiation radicals

$$R^{\bullet A} \xrightarrow{k_{d_A}} R^\bullet + R^{\bullet\bullet}$$

$$R^{\bullet B} \xrightarrow{k_{d_B}} R^\bullet + R^{\bullet\bullet}$$

in macroradicals

$$R_n^{\bullet A} \xrightarrow{k_{d_A}} R^\bullet + R_n^{\bullet\bullet} \qquad n = 1, ..., \infty$$

$$R_n^{\bullet B} \xrightarrow{k_{d_B}} R^\bullet + R_n^{\bullet\bullet} \qquad n = 1, ..., \infty$$

in temporary polymers

$$P_n^{\,A} \xrightarrow{k_{d_A}} R^\bullet + R_n^\bullet \qquad n = 1, ..., \infty$$

$$P_n^{\,B} \xrightarrow{k_{d_B}} R^\bullet + R_n^\bullet \qquad n = 1, ..., \infty$$

$$P_n^{\,AB} \xrightarrow{k_{d_A}} R^\bullet + R_n^{\bullet B} \qquad n = 2, ..., \infty$$

$$P_n^{\,AB} \xrightarrow{k_{d_B}} R^\bullet + R_n^{\bullet A} \qquad n = 2, ..., \infty$$

$$P_n^{\,AA} \xrightarrow{2k_{d_A}} R^\bullet + R_n^{\bullet A} \qquad n = 2, ..., \infty$$

$$P_n^{\,BB} \xrightarrow{2k_{d_B}} R^\bullet + R_n^{\bullet B} \qquad n = 2, ..., \infty$$

Initiation by Peroxide Radicals

$$R^\bullet + M \xrightarrow{k_i} R_1^\bullet$$

$$R^{\bullet A} + M \xrightarrow{k_i} R_1^{\bullet A}$$

$$R^{\bullet B} + M \xrightarrow{k_i} R_1^{\bullet B}$$

$$R^{\bullet\bullet} + M \xrightarrow{2k_i} R_1^{\bullet\bullet}$$

Thermal Initiation

$$3M \xrightarrow{k_{dm}} 2R_1^\bullet + M'$$

Propagation

$$R_n^\bullet + M \xrightarrow{k_p} R_{n+1}^\bullet \qquad n = 1, ..., \infty$$

$$R_n^{\bullet A} + M \xrightarrow{k_p} R_{n+1}^{\bullet A} \qquad n = 1, ..., \infty$$

$$R_n^{\bullet B} + M \xrightarrow{k_p} R_{n+1}^{\bullet B} \qquad n = 1, ..., \infty$$

$$R_n^{\bullet\bullet} + M \xrightarrow{2k_p} R_{n+1}^{\bullet\bullet} \qquad n = 1, ..., \infty$$

Chain Transfer to Monomer

$$R_n^\bullet + M \xrightarrow{k_{fm}} P_n + R_1^\bullet \qquad n = 1, ..., \infty$$

$$R_n^{\bullet A} + M \xrightarrow{k_{fm}} P_n^{\,A} + R_1^\bullet \qquad n = 1, ..., \infty$$

$$R_n^{\bullet B} + M \xrightarrow{k_{fm}} P_n^{\,B} + R_1^\bullet \qquad n = 1, ..., \infty$$

$$R_n^{\bullet\bullet} + M \xrightarrow{2k_{fm}} R_n^\bullet + R_1^\bullet \qquad n = 1, ..., \infty$$

Termination by Combination

$$R_n^\bullet + R_m^\bullet \xrightarrow{k_t} P_{n+m} \qquad n, m = 1, ..., \infty$$

$$R_n^\bullet + R_m^{\bullet A} \xrightarrow{k_t} P_{n+m}^{\,A} \qquad n, m = 1, ..., \infty$$

$$R_n^\bullet + R_m^{\bullet B} \xrightarrow{k_t} P_{n+m}^{\,B} \qquad n, m = 1, ..., \infty$$

$$R_n^\bullet + R_m^{\bullet\bullet} \xrightarrow{2k_t} R_{n+m}^\bullet \qquad n, m = 1, ..., \infty$$

$$R_n^{\bullet A} + R_m^{\bullet A} \xrightarrow{k_t} P_{n+m}^{\,AA} \qquad n, m = 1, ..., \infty$$

$$R_n^{\bullet A} + R_m^{\bullet B} \xrightarrow{k_t} P_{n+m}^{\,AB} \qquad n, m = 1, ..., \infty$$

$$R_n^{\bullet A} + R_m^{\bullet\bullet} \xrightarrow{2k_t} R_{n+m}^{\bullet A} \qquad n, m = 1, ..., \infty$$

$$R_n^{\bullet B} + R_m^{\bullet B} \xrightarrow{k_t} P_{n+m}^{\,BB} \qquad n, m = 1, ..., \infty$$

$$R_n^{\bullet B} + R_m^{\bullet\bullet} \xrightarrow{2k_t} R_{n+m}^{\bullet B} \qquad n, m = 1, ..., \infty$$

$$R_n^{\bullet\bullet} + R_m^{\bullet\bullet} \xrightarrow{4k_t} R_{n+m}^{\bullet\bullet} \qquad n, m = 1, ..., \infty$$

A gel effect correlation[43] for bulk styrene polymerization is used to account for the diffusion-controlled termination reactions at high monomer conversion. This correlation is shown in Table 5, together with the equation we propose for the initiation efficiency.

Perfect mixing is assumed for the reaction mixture and the cooling jacket. The resulting energy balances are shown in Table 5. In the energy balance equation for the reaction mixture, the enthalpy of the initiator inlet flows has been neglected because these flows are very small in comparison to the total mass of the reaction medium. It is important to remark that the dependence of the density[44] and specific heat[45] of the reaction mixture on temperature and/or conversion is considered in this model. The corresponding equations are also shown in Table 5. The reaction enthalpy,[45] jacket fluid density, and specific heat[46] values are reported in Table 6.

As the polymerization proceeds, the reaction mixture viscosity increases, causing a significant reduction in the heat-transfer coefficient. Despite this, some authors have used constant heat-transfer coefficients in their models.[47,48] In other works, the decrease of the heat-transfer coefficient with conversion has been modeled by means of different empirical correlations.[28,49−51] In this work, we proposed a linear dependence of h_i on

Table 2. Balances of the *a*th Moments of Macroradicals

$$\frac{1}{V}\frac{d(Y_a^{\bullet}V)}{dt} = 2k_{dm}M^3 + k_i R^{\bullet} M + k_{d_A} M_a^{A} + k_{d_B} M_a^{B} + k_p M \sum_{j=0}^{a} \binom{a}{j} Y_j^{\bullet} - k_p M Y_a^{\bullet} + k_{fm} M (Y_0^{\bullet} + Y_0^{\bullet A} + Y_0^{\bullet B} + 2Y_0^{\bullet\bullet}) + k_{fm} M (2Y_a^{\bullet\bullet} - Y_a^{\bullet}) - k_t Y_a^{\bullet} (Y_0^{\bullet} + Y_0^{\bullet A} + Y_0^{\bullet B} + 2Y_0^{\bullet\bullet}) + 2k_t \sum_{j=0}^{a} \binom{a}{j} Y_{a-j}^{\bullet} Y_j^{\bullet\bullet}$$

$$\frac{1}{V}\frac{d(Y_a^{\bullet A}V)}{dt} = k_i R^{\bullet A} M - k_{d_A} Y_a^{\bullet A} + k_{d_B} M_a^{AB} + 2k_{d_A} M_a^{AA} + k_p M \sum_{j=0}^{a} \binom{a}{j} Y_j^{\bullet A} - k_p M Y_a^{\bullet A} - k_{fm} M Y_a^{\bullet A} - k_t Y_a^{\bullet A} (Y_0^{\bullet} + Y_0^{\bullet A} + Y_0^{\bullet B} + 2Y_0^{\bullet\bullet}) + 2k_t \sum_{j=0}^{a} \binom{a}{j} Y_{a-j}^{\bullet A} Y_j^{\bullet\bullet}$$

$$\frac{1}{V}\frac{d(Y_a^{\bullet B}V)}{dt} = k_i R^{\bullet B} M - k_{d_B} Y_a^{\bullet B} + k_{d_A} M_a^{AB} + 2k_{d_B} M_a^{BB} + k_p M \sum_{j=0}^{a} \binom{a}{j} Y_j^{\bullet B} - k_p M Y_a^{\bullet B} - k_{fm} M Y_a^{\bullet B} - k_t Y_a^{\bullet B} (Y_0^{\bullet} + Y_0^{\bullet A} + Y_0^{\bullet B} + 2Y_0^{\bullet\bullet}) + 2k_t \sum_{j=0}^{a} \binom{a}{j} Y_{a-j}^{\bullet B} Y_j^{\bullet\bullet}$$

$$\frac{1}{V}\frac{d(Y_a^{\bullet\bullet}V)}{dt} = 2k_i R^{\bullet\bullet} M + k_{d_A} Y_a^{\bullet A} + k_{d_B} Y_a^{\bullet B} + 2k_p M \sum_{j=0}^{a} \binom{a}{j} Y_j^{\bullet\bullet} - 2k_p M Y_a^{\bullet\bullet} - 2k_{fm} M Y_a^{\bullet\bullet} - 2k_t Y_a^{\bullet\bullet} (Y_0^{\bullet} + Y_0^{\bullet A} + Y_0^{\bullet B} + 2Y_0^{\bullet\bullet}) + 2k_t \sum_{j=0}^{a} \binom{a}{j} Y_{a-j}^{\bullet\bullet} Y_j^{\bullet\bullet}$$

s.t. $Y_a^{\gamma}(0) = 0$

Table 3. Balances of the *a*th Moments of Polymers

$$\frac{1}{V}\frac{d(M_a^{A}V)}{dt} = -k_{d_A} M_a^{A} + k_{fm} M Y_a^{\bullet A} + k_t \sum_{j=0}^{a} \binom{a}{j} Y_{a-j}^{\bullet} Y_j^{\bullet A}$$

$$\frac{1}{V}\frac{d(M_a^{B}V)}{dt} = -k_{d_B} M_a^{B} + k_{fm} M Y_a^{\bullet B} + k_t \sum_{j=0}^{a} \binom{a}{j} Y_{a-j}^{\bullet} Y_j^{\bullet B}$$

$$\frac{1}{V}\frac{d(M_a^{AB}V)}{dt} = -(k_{d_A} + k_{d_B}) M_a^{AB} + k_t \sum_{j=0}^{a} \binom{a}{j} Y_{a-j}^{\bullet A} Y_a^{\bullet B}$$

$$\frac{1}{V}\frac{d(M_a^{AA}V)}{dt} = -2k_{d_A} M_a^{AA} + \frac{1}{2} k_t \sum_{j=0}^{a} \binom{a}{j} Y_{a-j}^{\bullet A} Y_j^{\bullet A}$$

$$\frac{1}{V}\frac{d(M_a^{BB}V)}{dt} = -2k_{d_B} M_a^{BB} + \frac{1}{2} k_t \sum_{j=0}^{a} \binom{a}{j} Y_{a-j}^{\bullet B} Y_j^{\bullet B}$$

$$\frac{1}{V}\frac{d(M_a V)}{dt} = k_{fm} M Y_a^{\bullet} + \frac{1}{2} k_t \sum_{j=0}^{a} \binom{a}{j} Y_{a-j}^{\bullet} Y_j^{\bullet}$$

s.t. $M_a^{\lambda}(0) = 0$

conversion that represents experimental data[50] appropriately. Considering that the dominant resistance to heat transfer is internal, a linear dependence is also obtained for the global heat-transfer coefficient (see Table 5).

Table 4. Mass Balances and Reaction Volume Equation

Monomer

$$\frac{1}{V}\frac{d(MV)}{dt} = -3k_{dm}M^3 - k_i(R^{\bullet} + R^{\bullet A} + R^{\bullet B} + 2R^{\bullet\bullet})M - k_{fm} M (Y_0^{\bullet} + Y_0^{\bullet A} + Y_0^{\bullet B} + 2Y_0^{\bullet\bullet}) - k_p M (Y_0^{\bullet} + Y_0^{\bullet A} + Y_0^{\bullet B} + 2Y_0^{\bullet\bullet}) \quad \text{s.t.} \quad M(0) = M_{t=0}$$

Initiators

$$\frac{1}{V}\frac{d(I_B V)}{dt} = -(k_{d_A} + k_{d_B}) I_B + \frac{F_{I_B}}{V} \quad \text{s.t.} \quad I_B(0) = I_{B0}$$

$$\frac{1}{V}\frac{d(I_{MA} V)}{dt} = -k_{d_A} I_{MA} + \frac{F_{I_{MA}}}{V} \quad \text{s.t.} \quad I_{MA}(0) = I_{MA0}$$

$$\frac{1}{V}\frac{d(I_{MB} V)}{dt} = -k_{d_B} I_{MB} + \frac{F_{I_{MB}}}{V} \quad \text{s.t.} \quad I_{MB}(0) = I_{MB0}$$

Initiation Radicals

$$\frac{1}{V}\frac{d(R^{\bullet A}V)}{dt} = f_B k_{d_B} I_B - k_{d_A} R^{\bullet A} - k_i R^{\bullet A} M$$

$$\frac{1}{V}\frac{d(R^{\bullet B}V)}{dt} = f_B k_{d_A} I_B - k_{d_B} R^{\bullet B} - k_i R^{\bullet B} M$$

$$\frac{1}{V}\frac{d(R^{\bullet\bullet}V)}{dt} = f_B (k_{d_A} R^{\bullet A} + k_{d_B} R^{\bullet B}) - 2k_i R^{\bullet\bullet} M$$

$$\frac{1}{V}\frac{d(R^{\bullet}V)}{dt} = f_B [(k_{d_A} + k_{d_B}) I_B + k_{d_A} R^{\bullet A} + k_{d_B} R^{\bullet B} + k_{d_A} (Y_0^{\bullet A} + M_0^{A} + M_0^{AB} + 2M_0^{AA}) + k_{d_B} (Y_0^{\bullet B} + M_0^{B} + M_0^{AB} + 2M_0^{BB})] + 2f_{MA} k_{d_A} I_{MA} + 2f_{MB} k_{d_B} I_{MB} - k_i R^{\bullet} M$$

s.t. $R^{\bullet A}(0) = R^{\bullet B}(0) = R^{\bullet}(0) = R^{\bullet\bullet}(0) = 0$

Reaction Mixture Volume

$$\frac{dV}{dt} = -\frac{\epsilon}{M_{t=0}} \frac{d(MV)}{dt} \quad \text{s.t.} \quad V(0) = V_0$$

3. Process and Control System Design Variables

The design objective consists of minimizing the batch time required to attain a given monomer conversion. At the same time, the final product must fulfill certain requirements with respect to the weight-average molecular weight (M_w) and polydispersity (Pd) ranges. The process design variables include the starting initiator mixture composition and initial concentration, the initial reaction temperature, and the reactor geometry. The control system design includes the optimal trajectories of the feedforward controllers, the selection of the optimal feedback control scheme from a control superstructure, the temperature set point of the feedback controller, and the tuning parameters of the feedback controller

Initiator Mixture Composition and Initial Concentration. In this work, we propose the selection of the optimum initiator mixture to accomplish a particular design objective. This involves deciding which peroxides to include in the starting initiator mixture (discrete decisions), and their initial concentrations. The mixture should contain at least one out of three different peroxides, one bifunctional (I_B) and two monofunctional (I_{MA} and I_{MB}). The bifunctional initiator is 4-(*tert*-butylperoxycarbonyl-3-hexyl-6-[7-(*tert*-butylperoxycarbonyl)heptyl]cyclohexene, which contains two peroxide groups (A and B).

Table 5. Energy Balances and Model Correlations[a]

	ref
Reaction Mixture Temperature	
$\frac{dT}{dt} = \frac{(-\Delta H)}{\rho C_p} k_p M(Y_0^{\bullet} + Y_0^{\bullet A} + Y_0^{\bullet B} + 2Y_0^{\bullet\bullet}) - \frac{UA}{\rho V C_p}(T - T_j) + \frac{H}{\rho V C_p}$	
s.t. $T(0) = T_0$	
Jacket Temperature	
$\frac{dT_j}{dt} = \frac{Q_j}{V_j}(T_{je} - T_j) - \frac{UA}{\rho_j V_j C_{pj}}(T_j - T)$	
s.t. $T_j(0) = T_{j0}$	
Density of the Reaction Mixture	
$\rho(\text{g L}^{-1}) = 1174 - 0.918T + (75.3 + 0.313T)\frac{\sum Y_1^{\gamma} + \sum M_1^{\lambda}}{M + \sum Y_1^{\gamma} + \sum M_1^{\lambda}}$	44
Specific Heat of the Reaction Mixture	
$C_p(\text{J g}^{-1}\text{ K}^{-1}) = 1.938 - 3.77 \times 10^{-3}T + 1.05 \times 10^{-5}T$	45
Dependence of the Heat-Transfer Coefficient on Conversion	
$U \approx h_i = h_{i,0}(1 - 0.7x)$	
Gel Effect Correlation	
$g \equiv \frac{k_t}{k_{t0}} = \exp[-2(Bx + Cx^2 + Dx^3)]$	43
$B = 2.57 - 5.05 \times 10^3 T$	28
$C = 9.56 - 1.76 \times 10^{-2} T$	28
$D = -3.03 + 7.85 \times 10^{-3} T$	28
Initiator Efficiency	
$f_B = f_{MA} = f_{MB} = 0.6807 - 18.2\left(I_{B0} + \frac{I_{MA0}}{2} + \frac{I_{MB0}}{2}\right)$	

[a] T in Kelvin.

Table 6. Kinetic Parameters and Initial Conditions[a]

	Kinetic Constants	ref
k_{d_A}	$1.04 \times 10^{15} \exp(-33500/RT)\ \text{s}^{-1}$	28
k_{d_B}	$8.06 \times 10^{13} \exp(-29800/RT)\ \text{s}^{-1}$	28
k_{dm}	$2.190 \times 10^5 \exp(-27440/RT)\ \text{s}^{-1}$	28
k_p	$1.051 \times 10^7 \exp(-7060/RT)\ \text{L mol}^{-1}\ \text{s}^{-1}$	28
k_{t0}	$1.260 \times 10^9 \exp(-1680/RT)\ \text{s}^{-1}$	28
$k_i \approx k_p$		28
k_{fm}	$7.807 \times 10^6 \exp(-12940/RT)\ \text{s}^{-1}$	28
	Initial Conditions	
V_0	1 L, 5000 L	
$M_{t=0}$	$8.728\ \text{mol L}^{-1}$	28
	Other Parameters	
ϵ	−0.147	28
$I_{B0,min} = I_{MA0,min} = I_{MB0,min}$	$0.001\ \text{mol L}^{-1}$	
$I_{B0,max} = I_{MA0,max} = I_{MB0,max}$	$0.01\ \text{mol L}^{-1}$	
ΔH	$-69919.56\ \text{J mol}^{-1}$	45
ρ_j	$1000\ \text{g L}^{-1}$	
C_{pj}	$4.1774\ \text{J g}^{-1}\text{ K}^{-1}$	46
$h_{i,0}$	$418\ \text{W K}^{-1}\text{ m}^{-2}$	

[a] R in cal/(mol K), T in Kelvin.

Peroxide group A presents a much slower decomposition rate than peroxide group B as a result of their different decomposition kinetic constants (see Table 6). For simplicity, the monofunctional initiators are assumed to be two hypothetical peroxides whose labile groups have decomposition rate constants equal to those of peroxide group A and peroxide group B, respectively, of the bifunctional initiator. As posed, the model can be easily extended to include any number of possible components of the initiator mixture.

The possibility of including initiators I_B, I_{MA}, and/or I_{MB} in the initiator mixture is modeled by the equations that specify their initial concentrations

$$I_{B0,min} y_B \le I_{B0} \le I_{B0,max} y_B \tag{5}$$

$$I_{MA0,min} y_{MA} \le I_{MA0} \le I_{MA0,max} y_{MA} \tag{6}$$

$$I_{MB0,min} y_{MB} \le I_{MB0} \le I_{MB0,max} y_{MB} \tag{7}$$

where y_B, y_{MA}, and y_{MB} are binary variables that take a value of 1 if their associated initiators are selected and 0 otherwise. Notice that these equations reduce to I_{B0}, I_{MA0}, or $I_{MB0} = 0$ if the corresponding binary variable is set to 0. An additional equation is added to specify that at least one initiator must be selected

$$y_B + y_{MA} + y_{MB} \ge 1 \tag{8}$$

Reactor Geometry. It is desired to find optimum reactor dimensions, i.e., reactor length and diameter, and reactor jacket volume. It is assumed that the reactor is a cylindrical vessel, with initial volume V_0 and heat-transfer area A given by eqs 9 and 10, respectively

$$V_0 = \frac{\pi}{4} D^2 L \tag{9}$$

$$A = \pi D L + \frac{\pi}{4} D^2 \tag{10}$$

A constant transfer area is assumed. Preliminary simulations with the process model indicated that this is a reasonable assumption, although this reaction exhibits volume contraction. Moreover, because we are considering a stirred reactor, the transfer area reduction becomes less important.

Two different reactor sizes are analyzed to study scale-up effects: a laboratory reactor of $V_0 = 1$ L and an industrial reactor of $V_0 = 5\ \text{m}^3$. Any given value of V_0 can be obtained with various combinations of reactor diameter D and height L, which results in different transfer areas according to eqs 9 and 10. As the transfer area plays a key role in reactor controllability,[28] it is important to find optimum values of D and L. The resulting dimensions must satisfy the constraint

$$^1/_3 \le \frac{D}{L} \le 2 \tag{11}$$

Finally, to obtain reasonable dimensions for the cooling jacket, it must be verified that

$$V_j \ge 0.1\ \text{L} \tag{12}$$

for the laboratory reactor and

$$V_j \ge 0.15\ \text{m}^3 \tag{13}$$

for the industrial reactor.

Control System Design. Feedforward controllers are used to keep the final M_w, Pd, and conversion within their constraints. Feedback and/or feedforward controllers are employed for reactor temperature control. All of the controllers are designed during the optimization process.

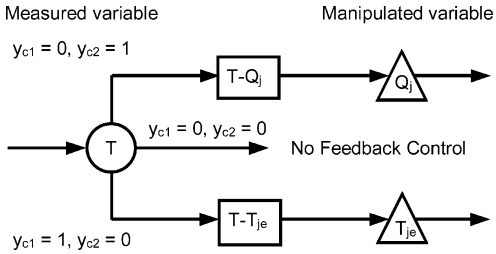

Figure 1. PI control superstructure.

The control variables of the feedforward controllers of M_w, Pd, and conversion are the inlet flows of the three peroxides to be added during the reaction (bifunctional, monofunctional A, and monofunctional B). These peroxides might be different from the ones present in the initial mixture. Their inlet flow rates $F_{I_B}(t)$, $F_{I_{MA}}(t)$, and $F_{I_{MB}}(t)$ are calculated as optimal piecewise-constant trajectories to minimize the objective function. These optimal trajectories are the corresponding feedforward controllers' actions.

Although the cooling jacket flow rate is usually manipulated for temperature control,[47] the coolant inlet temperature has also been used.[4,28,49] Hence, a control superstructure for a classical proportional-integral (PI) controller is proposed in which both alternatives are taken into account. Figure 1 presents that superstructure. In this figure, T is the reactor temperature, and Q_j and T_{je} are the coolant flow rate and inlet temperature, respectively. The binary variable y_{c1} takes a value of 1 if T_{je} is selected as the manipulated variable and 0 otherwise. The same applies to the binary variable y_{c2} associated with Q_j. The temperature set point (T_{set}) for the controllers is considered to be a time-varying control variable that is optimized as a series of piecewise-constant values. The design problem also involves optimizing the controller tuning parameters ($[K_{T_{je}},\tau_{T_{je}}]$ or $[K_{Q_j},\tau_{Q_j}]$), the nominal value of the manipulated variable (T_{jen} or Q_{jn}), and the time-invariant value of the variable that is not selected to be manipulated (T_{je} or Q_j).

The control superstructure for the PI controller is modeled by the following equations

$$T_{je} = T_{jen} + y_{c1}K_{T_{je}}\left(e + \frac{1}{\tau_{T_{je}}}\mathrm{IE}\right) \tag{14}$$

$$Q_j = Q_{jn} + y_{c2}K_{Q_j}\left(e + \frac{1}{\tau_{Q_j}}\mathrm{IE}\right) \tag{15}$$

$$e = T_{set} - T \tag{16}$$

$$\frac{\mathrm{d(IE)}}{\mathrm{d}t} = e \tag{17}$$

$K_{T_{je}}$ and $\tau_{T_{je}}$ are the gain and time constant, respectively, of the controller that manipulates T_{je}, and K_{Q_j} and τ_{Q_j} are the gain and time constant, respectively, of the controller that manipulates Q_j. Notice that, if T_{je} or Q_j is not selected as the manipulated variable ($y_{c1} = 0$ or $y_{c2} = 0$), the unselected variable becomes equal to the corresponding time-invariant value T_{jen} or Q_{jn}, respectively. The initial conditions for this set of equations are

$$\begin{aligned} e(0) &= 0 \\ \mathrm{IE}(0) &= 0 \end{aligned} \tag{18}$$

which imply that, at $t = 0$, $T = T_{set}$, $T_{je} = T_{jen}$, and $Q_j = Q_{jn}$. Notice that $T = T_{set}$ at the initial time means that the initial reaction temperature, T_0, which is part of the process design, becomes equal to the initial value of the optimization variable T_{set}.

As T_{je} and Q_j cannot be chosen simultaneously as the manipulated variable, the following integer constraint is considered

$$y_{c1} + y_{c2} \le 1 \tag{19}$$

An additional feedforward controller for temperature control is designed when the process has an extra heat supply. This additional controller's action is the trajectory for the heat supply, which is optimized as a series of piecewise-constant values.

Table 7. Simulation Results Using Our Previous Model[27] [a]

I_{B0} (mol/L)	T (°C)	batch time (min)	x	M_w	Pd
0.0042	80	400	0.35	317900	1.71
	90	400	0.71	387600	2.00
	100	328	**0.90**	**427000**	**2.17**
	110	400	1.00	406400	2.12
0.0084	80	400	0.50	281100	1.72
	90	400	1.00	348500	2.03
	100	400	1.00	339800	2.15
	110	400	1.00	339500	2.16

[a] The values in bold represent the single case in which the product specifications were satisfied before the final batch time.

4. Product Specifications and Process Constraints

It is desired to achieve a monomer conversion of at least 90%. At the same time, the product must satisfy certain quality requirements in terms of its weight-average molecular weight and polydispersity index. That is

$$x(t_f) \ge 0.9 \tag{20}$$

$$420000 \le M_w(t_f) \le 490000 \tag{21}$$

$$\mathrm{Pd}(t_f) \le 3 \tag{22}$$

These values were selected within the ranges commonly reported for styrene polymerization.

In a previous work, we addressed the mathematical modeling of this polymerization system, including validation against experimental data.[27] In that work, the bifunctional peroxide was the only initiator, and perfect isothermal operation was considered. We studied eight different combinations of initiator concentrations and temperatures, up to a batch time of 400 min. Table 7 shows simulation results for the eight sets of operating conditions, in terms of the product properties and process yield. Model parameters and remaining process conditions not shown in Table 7 can be found in ref 27. It can be seen that the product specifications required in the present study were simultaneously fulfilled before the final batch time in only one case. The process design obtained in the present work should reduce, if possible, the batch time needed to satisfy product demands.

Minimum and maximum values of the initiator concentrations shown in Table 6 were selected to keep process variables approximately in the ranges used in the model validation.[27]

The same reason motivated the selection of appropriate bounds on the reaction mixture temperature and the

temperature set point for the controller. These variables must be confined to the ranges

$$80\ °C \le T_{set}(t) \le 110\ °C \tag{23}$$

$$80\ °C \le T(t) \le 110\ °C \tag{24}$$

Constraints such as those shown in eq 24, which must be satisfied at every time t during the reaction, are dealt with by converting them into end-point constraints, that is, constraints that must be satisfied only at the final time, as described by eqs 25 and 26

$$T_{max}(t_f) \le 110\ °C \tag{25}$$

$$T_{min}(t_f) \ge 80\ °C \tag{26}$$

We employ the procedure developed by Bansal et al.[19] to track the maximum (or minimum) value over time of the variable on which the path constraint was defined, which results in eqs 27−30.

$$\frac{dT_{max}}{dt} = \frac{1}{4}\{1 + \tanh[10^6(T - T_{max})]\}\left[1 + \tanh\left(10^6 \frac{dT}{dt}\right)\right]\frac{dT}{dt} \tag{27}$$

$$\text{s.t.} \quad T(0) - T_{max}(0) = 0 \tag{28}$$

$$\frac{dT_{min}}{dt} = \frac{1}{4}\{1 - \tanh[10^6(T - T_{min})]\}\left[1 - \tanh\left(10^6 \frac{dT}{dt}\right)\right]\frac{dT}{dt} \tag{29}$$

$$\text{s.t.} \quad T(0) - T_{min}(0) = 0 \tag{30}$$

Water at atmospheric pressure was selected (in principle) as the jacket fluid. Thus, its temperature should not be higher than 100 °C. To maintain a safety margin, the following constraint must be satisfied

$$T_j(t) \le 95\ °C \tag{31}$$

This constraint is also converted to the end-point constraint shown in eq 32

$$T_{j,max}(t_f) \le 95\ °C \tag{32}$$

The application of the procedure of Bansal et al.[19] leads to the following equation that tracks the values of $T_{j,max}$ along the reaction time

$$\frac{dT_{j,max}}{dt} = \frac{1}{4}\{1 + \tanh[10^6(T_j - T_{j,max})]\}\left[1 + \tanh\left(10^6 \frac{dT_j}{dt}\right)\right]\frac{dT_j}{dt} \tag{33}$$

$$\text{s.t.} \quad T_j(0) - T_{j,max}(0) = 0 \tag{34}$$

We assume that the cooling water inlet temperature (T_{je}) cannot be colder than 7 °C. However, eq 14, which represents the feedback controller action on T_{je}, might yield values beyond this limit. To avoid violations on this bound, T_{je} can be represented by

$$T_{je} = \max(T_{je,FB}, 7) \tag{35}$$

where $T_{je,FB}$ is the feedback controller action on the coolant inlet temperature (eq 14). We propose eq 36 to smoothly approximate eq 35.

$$T_{je} = 0.5\{(T_{je,FB} - 7)\tanh[10^3(T_{je,FB} - 7)] + T_{je,FB} + 7\} \tag{36}$$

Minimum and maximum pump capacities determine that

$$1\ \frac{L}{min} \le Q_{jn} \le 10\ \frac{L}{min} \tag{37}$$

for the laboratory reactor and

$$90\ \frac{L}{min} \le Q_{jn} \le 2500\ \frac{L}{min} \tag{38}$$

for the industrial reactor.

5. Optimization Problem Formulation

The simultaneous design and control problem can be posed as follows

$$\begin{aligned} &\text{final batch time} = \min_{d,y,u(t)} t_f \\ &\text{s.t.} \\ &h_d(\dot{x}_d(t), x_d(t), x_a(t), u(t), d, p) = 0 \\ &h_a(x_d(t), x_a(t), u(t), d, y, p) = 0 \\ &h_0(\dot{x}_d(0), x_d(0), x_a(0), u(0), d, y, p) = 0 \\ &g_e(x_d(t_f), x_a(t_f)) \le 0 \\ &g_q(d, y, p) \le 0 \\ &g_y(y) \le 0 \\ &u^{lo} \le u(t) \le u^{up} \\ &d^{lo} \le d \le d^{up} \\ &y \in \{0, 1\}^5 \end{aligned} \tag{39}$$

where h_d is the set of differential equations (eqs 17, 29, 31, and 35 and the differential equations in Tables 2−5); h_a is the set of algebraic equations (eqs 1−3, 9, 10, 14−16, and 36 and the algebraic equations in Table 5; kinetic constant equations in Table 6; and monomer conversion definition); h_0 is the set of initial conditions; g_e is the set of end-point inequalities [eqs 20−22, 25, and 26 (and 32 if applicable)]; g_q is the set of time-invariant inequalities [eqs 5−7, 11−13, and 37 (or 38)]; g_y is the set of pure integer inequalities (eqs 8 and 19); u^{lo} and u^{up} are the sets of lower and upper bounds, respectively, on the manipulated variables; and d^{lo} and d^{up} are the sets of lower and upper bounds, respectively, on the design variables. In addition d represents the design variables (I_{B0}, I_{MA0}, I_{MB0}, L, V_j, T_{jen}, $K_{T_{je}}$, $\tau_{T_{je}}$, Q_{jn}, K_{Q_j}, τ_{Q_j}), y represents the binary variables (y_B, y_{MA}, y_{MB}, y_{c1}, y_{c2}), $x_d(t)$ represents the differential state variables (Y_a^{γ}, M_a^{λ}, M, $R^{\bullet A}$, $R^{\bullet B}$, $R^{\bullet}$, $R^{\bullet\bullet}$, I_B, I_{MA}, I_{MB}, V, T, T_j, T_{max}, T_{min}, $T_{j,max}$), $u(t)$ represents the manipulated (control) variables (F_{I_B}, $F_{I_{MA}}$, $F_{I_{MB}}$, T_{set}, H), $x_a(t)$ represents the algebraic variables (all other variables), and p represents the model parameters ($h_{i,0}$, V_0, $M_{t=0}$, ΔH, ρ_j, C_{pj},

preexponential factors and activation energies of kinetic constants, ϵ, $I_{B0,min}$, $I_{MA0,min}$, $I_{MB0,min}$, $I_{B0,max}$, $I_{MA0,max}$, $I_{MB0,max}$).

Equation 39 represents a MIDO problem. It should be noted that the differential-algebraic equation (DAE) system is a stiff, highly coupled and nonlinear system that turns the solution of the MIDO problem into a rather challenging task. Furthermore, because the system involves a polymerization reactor, it will be ill-conditioned because of the presence of very small and very large moments that describe the molecular weight distribution.

6. MIDO Problem Solution

The gPROMS v2.2.3 package (Process Systems Enterprise Ltd.) was used to solve the MIDO problem. The solution approach used by this software consists of the following features (i) A control vector parametrization expresses all time-varying optimization variables in terms of a finite set of time-invariant parameters. (ii) A mixed-integer nonlinear problem (MINLP) solver determines the optimal values of the optimization variables. (iii) A DAE solver is used to determine the values of all other variables, for any given set of the optimization variables, at the end of the time horizon.

gPROMS employs an OAERAP (outer approximation, equality relaxation, augmented penalty) solver [52−54] for the solution of the MINLP problem. Briefly, this is an iterative procedure in which the MINLP problem is decomposed into a "master" problem and a "primal" subproblem. In the latter, discrete variables remain fixed at their current values, and a nonlinear problem (NLP) solver is used to find the optimal values of the continuous optimization variables. In the master problem, the objective function and constraints carried out at the solutions of all continuous problems solved so far are linearized, and a mixed-integer linear problem (MILP) is solved, providing optimal values of both discrete and continuous optimization variables. The new values of the discrete variables are then used to solve the primal problem again, and the process is repeated until convergence is achieved.

To address the ill-conditioning of the problem, the scaling tool provided by the gPROMS solver was used on the optimization variables.

As was previously mentioned, solving MIDO optimization problems is a challenging task, particularly in the face of some complicating aspects involved in mathematical models of polymerization systems. Nevertheless, the software used allowed this difficult problem to be solved efficiently and reasonably free of trouble. As it is customary in this type of problem, an initial trial-an-error procedure had to be performed until a starting point was found. However, this was not too difficult as the starting point did not need to be too close to the optimal point for convergence to be achieved. Moreover, even when the optimization failed, the program provided information about the values of all optimization variables and constraints for the best available point obtained up to that moment, which proved to be of great help in improving the starting point.

7. Results and Discussion

Case A Design Problem. The simultaneous design and control problem as described before was considered for the laboratory-scale reactor without heat supply ($H = 0$). It involved 20 optimization variables, of which 5 are binary (y_B, y_{MA}, y_{MB}, y_{c1}, y_{c2}), 11 are time-invariant (design variables I_{B0}, I_{MA0}, I_{MB0}, L, V_j, T_{jen}, $K_{T_{je}}$, $\tau_{T_{je}}$, Q_{jn}, K_{Q_j}, τ_{Q_j}), and 4 are time-varying (manipulated variables F_{I_B}, $F_{I_{MA}}$, $F_{I_{MB}}$, T_{set}). The time horizon was divided into four time intervals to calculate optimal piecewise-constant profiles for the time-varying decision variables, namely, the temperature set point (T_{set}) and the inlet flows of the initiators F_{I_B}, $F_{I_{MA}}$, and $F_{I_{MB}}$. The optimizer calculated the optimal length of each time interval. Each of these intervals might take values from zero to the total batch time, subject to the condition that they should add up to the total batch time. The number of time intervals was fixed, but because the lengths in some could be zero, in practice, there could be fewer, so it was not necessary to consider a number of intervals greater than four.

Table 8. Optimal Process and Control Structure Design

objective function: final batch time (t_f)	352 min
reactor dimensions	
length	0.69 dm
diameter	1.36 dm
area	4.39 dm^2
cooling jacket volume	1 L
reaction mixture initial temperature	
$T_0 = T_{set}(0)$	95 °C
initiator mixture	
y_B	1
y_{MA}	0
y_{MB}	0
I_{B0}	0.00369 mol/L
I_{MA0}	0
I_{MB0}	0
initiator inlet flows	
$F_{I_B}(t)$	0
$F_{I_{MA}}(t)$	0
$F_{I_{MB}}(t)$	0
feedback control structure	
y_{c1}	0
y_{c2}	0
T_{jen}	94.8 °C
Q_{jn}	10 L/min

Table 8 reports the optimization results. The minimum batch time is 352 min. With our previous model,[27] we had obtained a shorter batch time that satisfied product specifications (see Table 7). However, in that case, the cooling system was different. It was assumed that an oil bath permitted isothermal operation at temperatures equal to and higher than 100 °C. As we show later, cooling fluid constraints play a key role in the behavior of this process.

It is interesting to note that the best policy for the peroxide inlet flows consists of no peroxide injection, that is, to operate the reactor in batch mode. Moreover, the optimally selected starting initiator mixture includes the bifunctional initiator only. As mentioned before, previous works have demonstrated the superiority of bifunctional initiators to monofunctional mixtures, but the performance of the combination of the two types of peroxides is not obvious and might depend on the features of the process at hand. Figure 2 depicts the initiator concentration profile. Note that the peroxide is used efficiently, as almost no initiator is present at the end of the reaction.

Figures 3−5 show the conversion, weight-average molecular weight, and polydispersity profiles, respectively. As can be observed, the product specifications are satisfied at the final batch time. The monomer conversion and M_w at the final time lie at their lower permitted

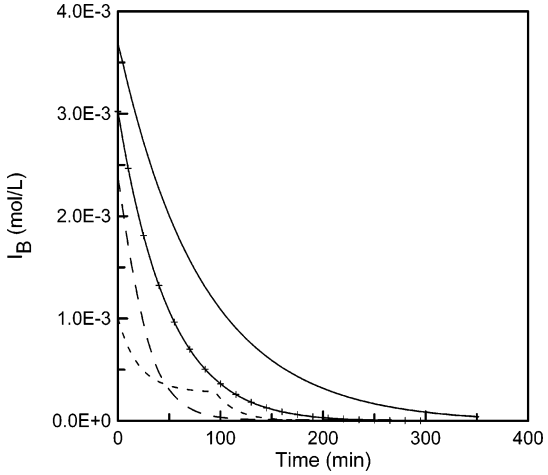

Figure 2. Bifunctional initiator concentration profiles for the different design cases: — case A, - - - case B, —+— case C, — — — case D.

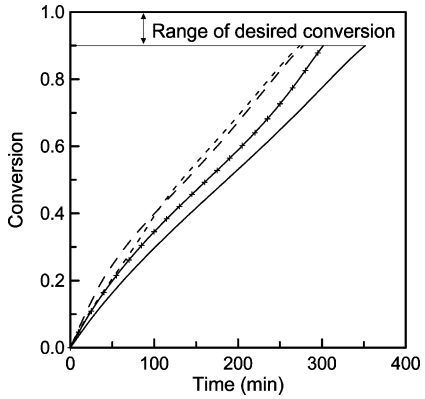

Figure 3. Conversion profiles for the different design cases: — case A, - - - case B, —+— case C, — — — case D.

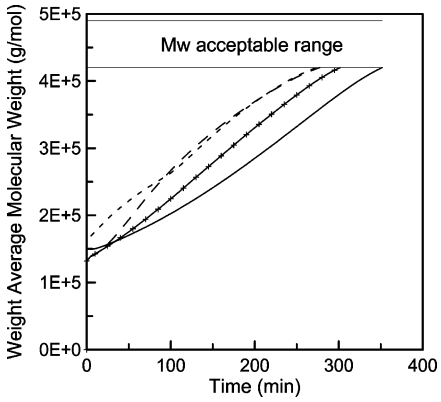

Figure 4. Weight-average molecular weight profiles for the different design cases: — case A, - - - case B, —+— case C, — — — case D.

values. This is an expected result, given that reducing batch time will reduce M_w and conversion. On the other hand, polydispersity is far from its upper bound.

The results in Table 8 indicate, surprisingly, that it is best not to incorporate any feedback loop to control the reactor temperature ($y_{c1} = 0$, $y_{c2} = 0$). The possible manipulated variables, T_{je} and Q_j, are then set to time-invariant values (T_{jen} and Q_{jn}, respectively), according to eqs 14 and 15. Figure 6 shows the reactor and jacket fluid temperatures. It can be observed that the temperature constraints are satisfied over the whole time horizon. Note that the cooling fluid temperature is

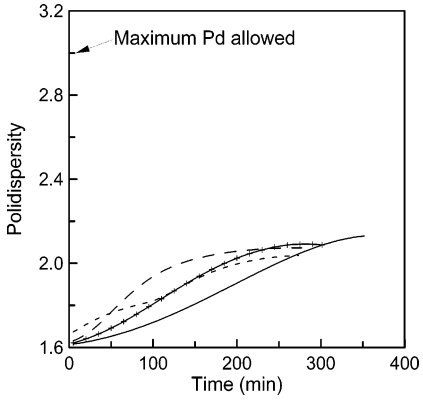

Figure 5. Polydispersity profiles for the different design cases: — case A, - - - case B, —+— case C, — — — case D.

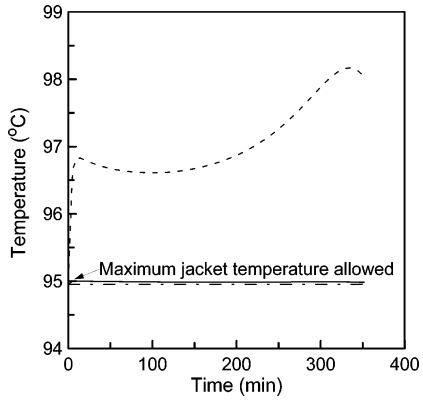

Figure 6. Temperature profiles for the case A design problem: - - - reactor temperature, — jacket fluid temperature, — - — jacket fluid inlet temperature.

almost constant at its maximum permitted value. In contrast, the reaction mixture temperature is far from its lower and upper bounds of 80 and 110 °C, respectively. The profile of this process variable also experiences very small variations, although no control action is being taken.

Table 9 lists the values of the constraint equations at the optimal point. It can be observed that the maximum jacket fluid temperature (eq 32) is, actually, an active constraint. In addition, the reactor dimensions found by the optimizer (see Table 8) result in a transfer area that is the minimum for a cylindrical vessel of 1 L. This information suggests that the optimizer determined a design such that the process can operate at the highest temperature compatible with the restriction imposed on the jacket temperature. To verify this conclusion, a second optimization run was performed in which the cooling fluid temperature constraint was not included. This would be the case if other coolants that can be used at higher temperatures, such as pressurized water, glycol mixtures, or Dowtherm, had been selected. (If a coolant other than water is selected, its specific physical properties should be considered, but because we are only interested in the effect of the maximum temperature restriction, we continue to use physical properties of water.) This design problem is called case B.

Case B Design Problem. Table 10 presents the optimal process and control design for case B. Table 11 shows the values of the constraint equations at the optimal point.

The minimum batch time in this case is 274 min. This means reductions of 22% with respect to the previous

Table 9. Constraint Values at the Optimal Solution of the Case A Design Problem

	constraint	value
eq 11	$^1/_3 \le D/L \le 2$	$^1/_3 \le 1.97 \le 2$
eq 12	$V_j \ge 0.1$ L	1 L $\ge$ 0.1 L
eq 37	1 L/min $\le Q_{jn} \le$ 10 L/min	1 L/min $\le$ 10 L/min $\le$ 10 L/min
eq 25	$T_{max}(t_f) \le 110$ °C	98 °C $\le$ 110 °C
eq 26	$T_{min}(t_f) \ge 80$ °C	95 °C $\ge$ 80 °C
eq 32	$T_{j,max}(t_f) \le 95$ °C	95 °C $\le$ 95 °C
eq 20	$x(t_f) \ge 0.9$	0.9 $\ge$ 0.9
eq 21	420000 g/mol $\le M_w(t_f) \le$ 490000 g/mol	420000 g/mol $\le$ 420000 g/mol $\le$ 490000 g/mol
eq 22	$Pd(t_f) \le 3$	2.1 $\le$ 3
eq 5	y_B0.001 mol/L $\le I_{B0} \le y_B$0.01 mol/L	0.001 mol/L $\le$ 0.00369 mol/L $\le$0.01 mol/L
eq 6	y_{MA}0.001 mol/L $\le I_{MA0} \le y_{MA}$0.01 mol/L	0 mol/L $\le$ 0 mol/L $\le$ 0 mol/L
eq 7	y_{MB}0.001 mol/L $\le I_{MB0} \le y_{MB}$0.01 mol/L	0 mol/L $\le$ 0 mol/L $\le$0 mol/L
eq 8	$y_B + y_{MA} + y_{MB} \ge 1$	1 $\ge$ 1
eq 19	$y_{c1} + y_{c2} \le 1$	0 $\le$ 1

Table 10. Optimal Process and Control Structure Design

objective function: final batch time (t_f)	274 min
reactor dimensions	
length	2.25 dm
diameter	0.75 dm
area	5.77 dm^2
cooling jacket volume	0.19 L
reaction mixture initial temperature	
$T_0 = T_{set}(0)$	108.7 °C
initiator mixture	
y_B	1
y_{MA}	0
y_{MB}	0
I_{B0}	0.001 mol/L
I_{MA0}	0
I_{MB0}	0
initiator inlet flows	
$0 \le t \le$ 32.7min	
$F_{I_B}(t)$	1.27 × 10^{-5} mol/min
$F_{I_{MA}}(t)$	0
$F_{I_{MB}}(t)$	0
32.7 min $< t \le$ 94.7 min	
$F_{I_B}(t)$	1.26 × 10^{-5} mol/min
$F_{I_{MA}}(t)$	0
$F_{I_{MB}}(t)$	0
94.7 min $< t \le$ 95.7 min	
$F_{I_B}(t)$	5.80 × 10^{-7} mol/min
$F_{I_{MA}}(t)$	1.60 × 10^{-7} mol/min
$F_{I_{MB}}(t)$	0
$t >$ 95.7 min	
$F_{I_B}(t)$	0
$F_{I_{MA}}(t)$	0
$F_{I_{MB}}(t)$	0
feedback control structure	
y_{c1}	0
y_{c2}	0
T_{jen}	107 °C
Q_{jn}	1.16 L/min

case and of 16% with respect to the batch time obtained in our previous work.[27] As in case A, no feedback loop is selected to control the reactor temperature. Nevertheless, the reactor operates almost isothermally, as Figure 7 illustrates. In fact, the temperature profiles are similar to those of case A, but displaced to higher levels. Now, the maximum reactor temperature is an active bound (see also eq 25 in Table 11).

The reactor transfer area is no longer the minimum possible area. This is an expected result because, with no upper bound on the jacket temperature, there is now no need to minimize the transfer area to allow the reactor temperature to be increased. This can now be achieved with a higher jacket temperature. This possibility allows for operation at a higher temperature range than in case A, reducing the necessary batch time.

From a practical point of view, the optimal selection for the initiator mixture includes, again, only the bifunctional peroxide in terms of both the initial concentrations in the reactor and the inlet flows (see Table 10). However, it can be seen that the optimization result yielded a nonzero flow of monofunctional initiator A at a certain time in the reaction. As shown later, this addition can be neglected. Figure 2 depicts the bifunctional initiator profile. The breaks in the curve clearly show the effect of the changes in the inlet flow. As in case A, no peroxide is present at the end of the reaction. The total amount of peroxide used was found to be 0.00220 mol in case B, compared to 0.00369 mol in case A. This amounts to a reduction of approximately 40% in the total peroxide used. The above quantities were calculated as the sum of the peroxide initially present and that added during the reaction.

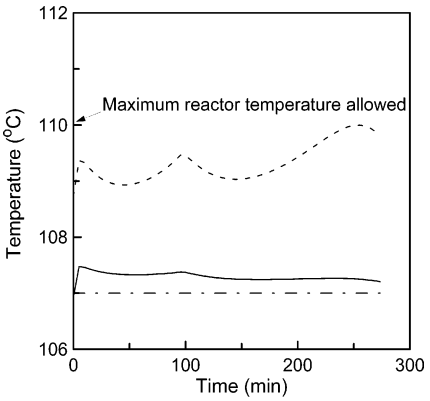

Figure 7. Temperature profiles for the case B design problem: - - - reactor temperature, — jacket fluid temperature, — - — jacket fluid inlet temperature.

The optimization results presented in Table 10 indicate that the monofunctional initiator A is added during a very short time of 1 min, corresponding to the third time period. The total number of moles of this initiator added is only 1.60 × 10^{-7}, which is negligible in comparison with the total amount of 0.00220 mol of peroxide used. Something similar occurs with the amount of bifunctional peroxide added in the third time period. To confirm that it is not necessary to make these additions, a simulation was performed with the case B optimal design features, but omitting peroxide addition after 94.7 min. As expected, equivalent results were obtained that differed by less than 0.1%.

Figures 3−5 illustrate the conversion, weight-average molecular weight, and polydispersity profiles. It is possible to observe that the product specifications are reached in a shorter time because of the relaxation of the upper limit of the jacket temperature.

Case C Design Problem. A design modification was analyzed for the case A design problem that consisted

Table 11. Constraint Values at the Optimal Solution of the Case B Design Problem

	constraint	value
eq 11	$^1/_3 \le D/L \le 2$	$^1/_3 \le {}^1/_3 \le 2$
eq 12	$V_j \ge 0.1$ L	0.19 L $\ge$ 0.1 L
eq 37	1 L/min $\le Q_{jn} \le$ 10 L/min	1 L/min $\le$ 1.16 L/min $\le$ 10 L/min
eq 25	$T_{max}(t_f) \le 110$ °C	110 °C $\le$110 °C
eq 26	$T_{min}(t_f) \ge 80$ °C	108.7 °C $\ge$ 80 °C
eq 20	$x(t_f) \ge 0.9$	0.9 $\ge$ 0.9
eq 21	420000 g/mol $\le M_w(t_f) \le$ 490000 g/mol	420000 g/mol $\le$ 420000 g/mol $\le$ 490000 g/mol
eq 22	$Pd(t_f) \le 3$	2.0 $\le$ 3
eq 5	y_B0.001 mol/L $\le I_{B0} \le y_B$0.01 mol/L	0.001 mol/L $\le$ 0.001 mol/L $\le$ 0.01 mol/L
eq 6	y_{MA}0.001 mol/L $\le I_{MA0} \le y_{MA}$0.01 mol/L	0 mol/L $\le$ 0 mol/L $\le$ 0 mol/L
eq 7	y_{MB}0.001 mol/L $\le I_{MB0} \le y_{MB}$0.01 mol/L	0 mol/L $\le$ 0 mol/L $\le$ 0 mol/L
eq 8	$y_B + y_{MA} + y_{MB} \ge 1$	1 $\ge$ 1
eq 19	$y_{c1} + y_{c2} \le 1$	0 $\le$ 1

Table 12. Optimal Process and Control Structure Design

objective function: final batch time (t_f)	302 min
reactor dimensions	
length	1.32 dm
diameter	0.98 dm
area	4.83 dm^2
cooling jacket volume	0.39 L
reacting mixture initial temperature	
$T_0 = T_{set}(0)$	101 °C
initiator mixture	
y_B	1
y_{MA}	0
y_{MB}	0
I_{B0}	0.00302 mol/L
I_{MA0}	0
I_{MB0}	0
initiator inlet flows	
$0 \le t \le 0.031$ min	
$F_{I_B}(t)$	6.55×10^{-7} mol/min
$F_{I_{MA}}(t)$	0
$F_{I_{MB}}(t)$	1.15×10^{-6} mol/min
$t > 0.031$ min	
$F_{I_B}(t)$	0
$F_{I_{MA}}(t)$	0
$F_{I_{MB}}(t)$	0
heat load	
$0 \le t \le 0.031$ min	
$H(t)$	149 W
$t > 0.031$ min	
$H(t)$	84 W
feedback control structure	
y_{c1}	0
y_{c2}	0
T_{jen}	94.8 °C
Q_{jn}	10 L/min

in adding a heat supply to the reactor. This combination of heat load−reactor cooling has been used in experimental works dealing with styrene polymerization.[50] The heat supply to the reactor is considered to be manipulated by a feedforward controller. An optimal heat load profile [$H(t)$] must now be determined as part of the reactor design.

The optimal process and control design for case C is shown in Table 12, and the values of the constraint equations at the optimal point can be found in Table 13. It is interesting to see that the heat addition reduces the minimum batch time by 50 min with respect to case A. As Figure 8 illustrates, the jacket temperature lies almost at its upper bound during the whole reaction, as in case A, so as to allow the highest possible reactor temperature. However, with the added heat, the reactor temperature can reach higher levels, thus reducing the necessary reaction time. Another consequence of the heat addition is that it is no longer necessary to minimize heat transfer as in case A. That is why the transfer area is now greater than the minimum area, as Table 12 shows.

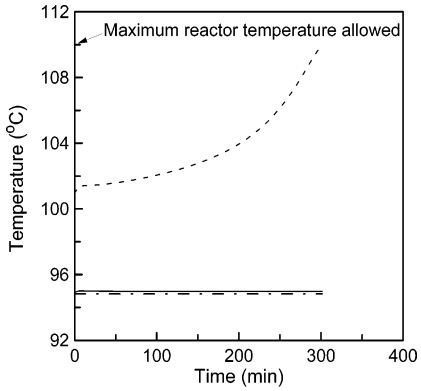

Figure 8. Temperature profiles for the case C design problem: - - - reactor temperature, — jacket fluid temperature, — - — jacket fluid inlet temperature.

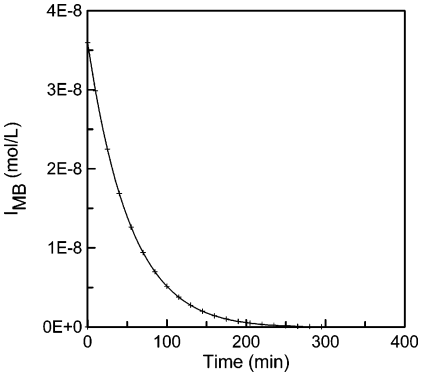

Figure 9. Monofunctional B concentration profile for the case C design problem.

Only the bifunctional initiator, as in cases A and B, is used in the initial initiator mixture. An addition of the bifunctional initiator is employed at the early stages of the reaction. It is interesting to see that, unlike the previous cases, an addition of the monofunctional initiator B together with the bifunctional initiator is employed (see Table 12). However, the period of peroxide addition is very short and their flow rates are very low. Figures 2 and 9 depict the bifunctional and monofunctional B initiator profiles, respectively. It can be seen that both peroxides are completely consumed in the reaction. The amount of initiator used is greater than in case B, but smaller than in case A. It can easily be calculated that the bifunctional initiator consumption is 0.00302002 mol, while the monofunctional B initiator consumption is 3.5×10^{-8} mol.

The total amount of initiators added during the reaction is insignificant, on the order of 10^{-8} mol. A similar situation was found in case B with the addition of peroxides in the third time interval. Again, to confirm

Table 13. Constraint Values at the Optimal Solution of the Case C Design Problem

	constraint	value
eq 11	$^1/_3 \le D/L \le 2$	$^1/_3 \le 0.75 \le 2$
eq 12	$V_j \ge 0.1$ L	0.39 L $\ge$ 0.1 L
eq 37	1 L/min $\le Q_{jn} \le$ 10 L/min	1 L/min $\le$ 10 L/min $\le$ 10 L/min
eq 25	$T_{max}(t_f) \le$ 110 °C	110 °C $\le$ 110 °C
eq 26	$T_{min}(t_f) \ge$80 °C	101 °C $\ge$ 80 °C
eq 32	$T_{j,max}(t_f) \le$ 95 °C	95 °C $\le$ 95 °C
eq 20	$x(t_f) \ge 0.9$	0.9 $\ge$ 0.9
eq 21	420000 g/mol $\le M_w(t_f) \le$ 490000 g/mol	420000 g/mol $\le$ 420000 g/mol $\le$ 490000 g/mol
eq 22	$Pd(t_f) \le 3$	2.1 $\le$ 3
eq 5	y_B0.001 mol/L $\le I_{B0} \le y_B$0.01 mol/L	0.001 mol/L $\le$ 0.00302 mol/L $\le$ 0.01 mol/L
eq 6	y_{MA}0.001 mol/L $\le I_{MA0} \le y_{MA}$0.01 mol/L	0 mol/L $\le$ 0 mol/L $\le$ 0 mol/L
eq 7	y_{MB}0.001 mol/L $\le I_{MB0} \le y_{MB}$0.01 mol/L	0 mol/L $\le$ 0 mol/L $\le$ 0 mol/L
eq 8	$y_B + y_{MA} + y_{MB} \ge 1$	1 $\ge$ 1
eq 19	$y_{c1} + y_{c2} \le 1$	0 $\le$ 1

Table 14. Optimal Process and Control Structure Design

objective function: final batch time (t_f)	277 min
reactor dimensions	
length	1.88 m
diameter	1.84 m
area	13.5 m^2
cooling jacket volume	4.3 m^3
reacting mixture initial temperature	
$T_0 = T_{set}(0)$	102 °C
initiator mixture	
y_B	1
y_{MA}	0
y_{MB}	0
I_{B0}	0.00238 mol/L
I_{MA0}	0
I_{MB0}	0
initiator inlet flows	
$0 \le t \le$ 5.6 min	
$F_{I_B}(t)$	0
$F_{I_{MA}}(t)$	0
$F_{I_{MB}}(t)$	0
$t >$ 5.6 min	
$F_{I_B}(t)$	0.002mol/min
$F_{I_{MA}}(t)$	0
$F_{I_{MB}}(t)$	0
feedback control structure	
y_{c1}	1
y_{c2}	0
T_{jen}	95 °C
$K_{T_{je}}$	12
$\tau_{T_{je}}$	13.95 min
Q_{jn}	554 L/min
$0 \le t \le$ 1.8 min	
$T_{set}(t)$	102 °C
1.8 min $\le t \le$ 5.6 min	
$T_{set}(t)$	80 °C
$t >$ 5.6 min	
$T_{set}(t)$	109.5 °C

that it is not necessary to make this negligible addition, a simulation was performed with the case C optimal design features but omitting peroxide addition after the reaction start. Almost the same results were obtained, presenting only negligible differences in the numerical values of the calculated variables: for instance, temperature values agree up to the third decimal place and conversion up to the fifth decimal place.

As in the previous cases, no feedback control is selected. Conversion, weight-average molecular weight, and polydispersity profiles are similar to those obtained for cases A and B, as can be seen in Figures 3−5.

Case D Design Problem. Table 14 presents the results for the design of the industrial-size reactor, called case D. Table 15 reports the constraint values at the optimal point. Water is used as the refrigerant, so eq 32 applies. Some coincidences can be found with respect to the laboratory reactor design. For instance, only the bifunctional initiator is used, with an initial

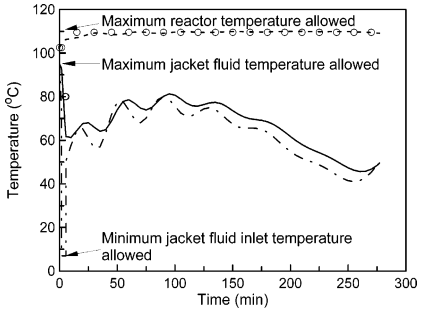

Figure 10. Temperature profiles for the case D design problem: - - - reactor temperature, — jacket fluid temperature, — - — jacket fluid inlet temperature, ○ temperature set point.

concentration similar to that used in case B. In addition, the conversion and M_w lie at their lowest acceptable values. On the other hand, significant differences appear in this case. For instance, feedback temperature control action is selected, for which T_{je} is chosen as the manipulated variable. As pointed out by Kim,[28] the poorer heat removal of industrial reactors compared to laboratory-scale reactors makes operation control much more difficult in the former case. This observation is in accordance with our result that the laboratory reactor can be feasibly operated in an open loop whereas the industrial reactor requires feedback control. Another difference is that an extra flow of bifunctional initiator is needed through most of the reaction time.

Figure 10 depicts the reactor temperature, reactor temperature set point, manipulated variable (T_{je}), and jacket fluid temperature trajectories corresponding to the case D design. It can be seen that the reactor operates almost isothermally at approximately 110 °C (the reactor temperature upper bound), closely following its set-point value. Because of the smaller heat-transfer capacity of the industrial reactor, it is now possible to operate at this temperature level without violating the maximum jacket fluid temperature. Notice that the average reactor temperature level is similar to that of case B, which yielded a similar reaction time.

Another difference with respect to case A is that the transfer area is no longer the minimum for the given volume. Now, the transfer area is 5% larger than its minimum possible value.

Figure 2 shows the peroxide concentration profile for case D. As in the previous cases, no peroxide is present at the end of the reaction. However, the initiator is more rapidly consumed in this instance.

The conversion, average molecular weights, and polydispersity present similar time profiles as in the previous cases (see Figures 3−5).

Table 15. Constraint Values at the Optimal Solution of the Case D Design Problem

	constraint	value
eq 11	$^1/_3 \le D/L \le 2$	$^1/_3 \le 0.98 \le 2$
eq 13	$V_j \ge 0.15$ m^3	4.3 m$^3 \ge 0.15$ m^3
eq 38	90 L/min $\le Q_{jn} \le$ 2500 L/min	90 L/min $\le$ 554 L/min $\le$ 2500 L/min
eq 25	$T_{max}(t_f) \le 110$ °C	110 °C $\le$ 110 °C
eq 26	$T_{min}(t_f) \ge 80$ °C	101.5 °C $\ge$ 80 °C
eq 32	$T_{j,max}(t_f) \le 95$ °C	95 °C $\le$ 95 °C
eq 20	$x(t_f) \ge 0.9$	$0.9 \ge 0.9$
eq 21	420000 g/mol $\le M_w(t_f) \le$ 490000 g/mol	420000 g/mol $\le$ 420000 g/mol $\le$ 490000 g/mol
eq 22	$Pd(t_f) \le 3$	$2.1 \le 3$
eq 5	y_B0.001 mol/L $\le I_{B0} \le y_B$0.01 mol/L	0.001 mol/L $\le$ 0.00238 mol/L $\le$ 0.01 mol/L
eq 6	y_{MA}0.001 mol/L $\le I_{MA0} \le y_{MA}$0.01 mol/L	0 mol/L $\le$ 0 mol/L $\le$ 0 mol/L
eq 7	y_{MB}0.001 mol/L $\le I_{MB0} \le y_{MB}$0.01 mol/L	0 mol/L $\le$ 0 mol/L $\le$ 0 mol/L
eq 8	$y_B + y_{MA} + y_{MB} \ge 1$	$1 \ge 1$
eq 19	$y_{c1} + y_{c2} \le 1$	$1 \le 1$

8. Conclusions

Simultaneous process and control designs were performed for industrial- and laboratory-scale semibatch bulk styrene polymerization systems. The integration of process and control system designs allowed optimum process designs to be obtained that are also controllable under the assumptions of no perturbations or model uncertainty. Feasible operations have been guaranteed in this way.

We showed the potential of the MIDO approach, as a relatively new tool in polymerization engineering, to uncover complex design and control decision interactions and provide insight into an integrated design methodology for industrial polymerization reactors. Results in our work clearly show that the use of an integrated and systematic methodology to incorporate control decisions early into the design problem of styrene polymerization reactors provides a better global understanding of the system interactions, resulting in an improved design and unit operation.

The MIDO approach permitted the achievement of an optimum design in a single optimization run using a comprehensive dynamic model of the process. The rigorous dynamic simulation included in the solution of the MIDO enables verification that process path and end-point constraints are satisfied. Discrete decisions such as the selection of initiators and the selection of the manipulated variable for a PI controller, have been successfully included in the optimization problem. The gPROMS/gOPT package was effectively applied to solve the mixed-integer dynamic optimization.

Optimal process and control system designs are obtained for a laboratory reactor but with different options for the control system (i.e., water as the coolant in the first case, a high-temperature coolant in the second, a heat supply in the third). Insight is gained by seeing how the optimal process design is different in each case, because of the influence of the different options available to control it. In the industrial reactor design, the control options available are the same as for case A of the laboratory reactor. However, owing to scale-up effects, a very different process and control system design is obtained.

Comparison of the results obtained for the industrial and laboratory reactors provides much insight into potential scale-up problems. For the latter reactor, optimal designs tended to minimize heat transfer between reaction mixture and cooling fluid to keep the temperature as high as possible, which reduces the reaction time. In this way, use of a high-temperature coolant or a heat supply helped to achieve a shorter batch time. Laboratory-scale reactors could be optimally operated without temperature control. In contrast, the industrial reactor needed appropriate heat removal to maintain feasible operation. Feedback temperature control was included in the optimal design in this case, with the coolant inlet temperature selected as the manipulated variable for the PI controller.

The bifunctional initiator was selected instead of monofunctional ones or mixtures of bi- and monofunctional initiators in all design cases analyzed. However, this result might be different for other lists of available initiators.

All of the examples presented in this work show the strong interaction that can exist between the process design and control of polymerization reactors.

The design approach presented here can easily be extended to other polymerization systems.

Acknowledgment

The authors thank CONICET and UNS for financial support.

Nomenclature

A = transfer area
C_p = specific heat of the reaction mixture
C_{pj} = specific heat of the coolant
d = set of design variables
D = reactor inside diameter
d^{lo} = set of lower bounds on the design variables
d^{up} = set of upper bounds on the design variables
e = error in the feedback temperature controller
f_B = efficiency of the bifunctional initiator
F_{I_B} = molar inlet flow of peroxide I_B
$F_{I_{MA}}$ = molar inlet flow of peroxide I_{MA}
$F_{I_{MB}}$ = molar inlet flow of peroxide I_{MB}
f_{MA} = efficiency of the monofunctional initiator with a peroxide A group
f_{MB} = efficiency of the monofunctional initiator with a peroxide B group
g_e = set of end-point inequalities
g_q = set of time-invariant inequalities
g_y = set of pure integer inequalities
H = heat load
h_0 = set of initial condition equations
h_a = set of algebraic equations
h_d = set of differential equations
h_i = inside heat-transfer coefficient
$h_{i,0}$ = inside heat-transfer coefficient at zero conversion
I_B = bifunctional peroxide initiator
I_{B0} = initial concentration of the bifunctional peroxide initiator

$I_{B0,max}$ = upper bound on the initial concentration of the bifunctional peroxide initiator
$I_{B0,min}$ = lower bound on the initial concentration of the bifunctional peroxide initiator
I_{MA} = monofunctional initiator with a peroxide A group
I_{MA0} = initial concentration of the monofunctional initiator with a peroxide A group
$I_{MA0,max}$ = upper bound on the initial concentration of the monofunctional initiator with a peroxide A group
$I_{MA0,min}$ = lower bound on the initial concentration of the monofunctional initiator with a peroxide A group
I_{MB} = monofunctional initiator with a peroxide B group
I_{MB0} = initial concentration of the monofunctional initiator with a peroxide B group
$I_{MB0,max}$ = upper bound on the initial concentration of the monofunctional initiator with a peroxide B group
$I_{MB0,min}$ = lower bound on the initial concentration of the monofunctional initiator with a peroxide B group
IE = integral of the error in the feedback temperature controller
k_{d_A} = kinetic constant for the peroxide A group decomposition reaction
k_{d_B} = kinetic constant for the peroxide B group decomposition reaction
k_{dm} = kinetic constant for the monomer thermal initiation reaction
k_{fm} = kinetic constant for the transfer to monomer reaction
k_i = kinetic constant for the initiation by peroxide radical reaction
k_p = kinetic constant for the propagation reaction
k_t = kinetic constant for the termination reaction
k_{t0} = kinetic constant for the termination reaction at zero conversion
$K_{T_{je}}$ = gain of the controller that manipulates the coolant inlet temperature
K_{Q_j} = gain of the controller that manipulates the coolant flow rate
M = monomer
M_{mon} = monomer molecular weight
M_a^{λ} = ath (a = 0, 1, 2) moment of polymer species with end-unit type λ
M_n = number-average molecular weight
$M_{t=0}$ = initial monomer concentration
M_w = weight-average molecular weight
Pd = polydispersity index
PI = proportional integral
P_n^{λ} = temporary polymer of chain length n with end-unit type λ
Q_j = coolant flow rate
Q_{jn} = nominal value of the coolant flow rate
$R^{\bullet}$ = initiation radical with a single active center
$R^{\bullet A}$ = initiation radical with a single active center and an undecomposed peroxide A group
$R^{\bullet B}$ = initiation radical with a single active center and an undecomposed peroxide B group
$R^{\bullet\bullet}$ = initiation radical with two active centers
R_n^{γ} = macroradical of chain length n with end-unit type γ
t = reaction time
t_f = final batch time
T = reactor temperature
T_0 = initial reactor temperature
T_j = jacket temperature
T_{j0} = initial jacket temperature
T_{je} = coolant inlet temperature
T_{jen} = nominal value of the coolant inlet temperature
$T_{je,FB}$ = feedback controller action on the coolant inlet temperature
$T_{j,max}(t)$ = maximum value of the jacket temperature in the interval [0, t]
$T_{max}(t)$ = maximum value of the reactor temperature in the interval [0, t]
$T_{min}(t)$ = minimum value of the reactor temperature in the interval [0, t]
T_{set} = reactor temperature set point
U = global heat-transfer coefficient
u^{lo} = set of lower bounds on the manipulated variables
u^{up} = set of upper bounds on the manipulated variables
$u(t)$ = set of manipulated variables
V = reactor volume
V_0 = initial reactor volume
V_j = jacket volume
x = monomer conversion
y = set of binary variables
y_B = binary variable associated with the use of the bifunctional initiator in the starting initiator mixture
y_{c1} = binary variable associated with the use of the coolant inlet temperature as the manipulated variable for the feedback controller
y_{c2} = binary variable associated with the use of the coolant flow rate as the manipulated variable for the feedback controller
y_{MA} = binary variable associated with the use of the monofunctional initiator with a peroxide A group in the starting initiator mixture
y_{MB} = binary variable associated with the use of the monofunctional initiator with a peroxide B group in the starting initiator mixture
Y_a^{γ} = ath (a = 0, 1, 2) moment of macroradical species with end-unit type γ

Greek symbols

ϵ = volume contraction factor
ρ = reaction mixture density
ρ_j = coolant density
ΔH = propagation reaction enthalpy
$\tau_{T_{je}}$ = time constant for the controller that manipulates the coolant inlet temperature
τ_{Q_j} = time constant for the controller that manipulates the coolant flow rate

Superscripts

A = end unit with an undecomposed peroxide A group
B = end unit with an undecomposed peroxide B group
$\bullet$ = end unit with a radical active center
$\bullet$A = one end unit with a radical active center and the other with an undecomposed peroxide A group
$\bullet$B = one end unit with a radical active center and the other with an undecomposed peroxide B group
$\bullet\bullet$ = two end units with radical active centers
γ = end-unit type $\bullet$, $\bullet\bullet$, $\bullet$A, or $\bullet$B
λ = end-unit type A, B, AA, BB, AB, or permanent polymer (no superscript)

Literature Cited

(1) Vogl, O.; Jaycox, G. D. Trends in Polymer Science. Polymer Science in the 21st Century. *Prog. Polym. Sci.* **1999**, *24*, 3.

(2) Rosen, S. L. *Fundamental Principles of Polymeric Materials for Practicing Engineers*; John Wiley & Sons: New York, 1993.

(3) Brydson, J. A. *Flow Properties of Polymer Melts*; Van Nostrand Reinhold Company: New York, 1970.

(4) Ogunnaike, B. A.; Ray, W. H. *Process Dynamics, Modeling, and Control*; Oxford University Press: New York, 1994.

(5) Ray, W. H.; Villa, C. M. Nonlinear Dynamics Found in Polymerization Processes—A Review. *Chem. Eng. Sci.* **1999**, *55*, 275.

(6) Bequette, B. W. Nonlinear Control of Chemical Processes: A Review. *Ind. Eng. Chem. Res.* **1991**, *30*, 1391.

(7) Congalidis, J. P.; Richards, J. R. Process Control of Polymerization Reactors: An Industrial Perspective. *Polym. React. Eng.* **1998**, *6*, 71.

(8) Schildknecht, C. E.; Skeist, I. *Polymerization Processes*; John Wiley & Sons: New York, 1977.

(9) Kiparissides, C. Polymerization Reactor Modeling: A Review of Recent Developments and Future Directions. *Chem. Eng. Sci.* **1996**, *51*, 1637.

(10) Embiruçu, M.; Lima, E. L.; Pinto, J. C. A Survey of Advanced Control of Polymerization Reactors. *Polym. Eng. Sci.* **1996**, *36*, 433.

(11) MacGregor, J. F.; Penlidis, A.; Hamielec, A. E. Control of Polymerization Reactors: A Review. *Polym. Process Eng.* **1984**, *2*, 179.

(12) Crowley T. J.; Choi, K. Y. Discrete Optimal Control of Molecular Weight Distribution in a Batch Free Radical Polymerization Process. *Ind. Eng. Chem. Res.* **1997**, *36*, 3676.

(13) Tieu, D.; Cluett, W. R.; Penlidis, A. Optimization of Polymerization Reactor Operation: Review and Case Studies with the End-Point Collocation Method. *Polym. React. Eng.* **1994**, *2*, 275.

(14) Crowley T. J.; Choi, K. Y. Control of Molecular Weight Distribution and Tensile Strength in a Free Radical Styrene Polymerization Process. *J. Appl. Polym. Sci.* **1998**, *70*, 1017.

(15) Rafizadeh, M. Sequential Linearization Adaptive Control of Solution Polymerization of Methyl Methacrylate in a Batch Reactor. *Polym. React. Eng.* **2002**, *10*, 121.

(16) Yabuki, Y.; Nagasawa, T.; MacGregor, J. F. Industrial Experiences with Product Quality Control in Semi-Batch Processes. *Comput. Chem. Eng.* **2002**, *26*, 205.

(17) Grossmann, I. E.; Morari, M. Operability, Resilience and Flexibility: Process Design Objectives for a Changing World. In *Proceedings of the 2nd International Conference on Foundations of Computer Aided Process Design, FOCAPD-1983*; Westerberg, A. W., Chien, H. N., Eds.; CACHE/AIChE: New York, 1984; p 931.

(18) Ziegler, J. G.; Nichols, N. B. Process Lags in Automatic Control Circuits. *Trans. ASME* **1943**, *65*, 433.

(19) Bansal, V.; Perkins, J. D.; Pistikopoulos, E. N. A Case Study in Simultaneous Design and Control Using Rigorous, Mixed-Integer Dynamic Optimization Models. *Ind. Eng. Chem. Res.* **2002**, *41*, 760.

(20) Morari, M.; Perkins, J. Design for Operations. In *Proceedings of the 4th International Conference on Foundations of Computer Aided Process Design, FOCAPD-1994*; Biegler, L. T., Doherty, M. F., Eds.; CACHE/AIChE: New York, 1995; p 105.

(21) Navarray, L. T.; Perkins, J. D. Selection of Control Structure Based on Linear Dynamic Economics. *Ind. Eng. Chem. Res.* **1993**, *32*, 2681.

(22) Bahri, P.; Bandoni, A.; Romagnoli, J. Integrated Flexibility and Controllability Analysis in Design of Chemical Processes. *AIChE J.* **1997**, *43*, 997.

(23) Mohideen, M.; Perkins, J.; Pistikopoulos, E. N. Optimal Design of Dynamic Systems under Uncertainty. *AIChE J.* **1996**, *42*, 2251.

(24) Perkins, J.; Walsh, S. Optimization as a Tool for Design/Control Integration. *Comput. Chem. Eng.* **1996**, *20*, 315.

(25) van Schijndel, J. M. G.; Pistikopoulos, E. N. Towards the Integration of Process Design, Process Control and Process Operability—Current Status and Futures Trends. In *Proceedings of the 5th International Conference on Foundations of Computer Aided Process Design, FOCAPD-1999*; Malone, M. F., Trainham, J. A., Carnahan, B., Eds. CACHE/AIChE: New York, 1999; p 99.

(26) Chatzidoukas, C.; Perkins, J. D.; Pistikopoulos, E. N.; Kiparissides, C. Optimal Grade Transition and Selection of Closed-Loop Controllers in a Gas-Phase Olefin Polymerization Fluidized Bed Reactor. *Chem. Eng. Sci.* **2003**, *58*, 3643.

(27) Asteasuain, M.; Brandolin, A.; Sarmoria, C. Molecular Weight Distributions in Styrene Polymerization with Asymmetric Bifunctional Initiators. *Polymer* **2004**, *45*, 321.

(28) Kim, K. J. Modeling and Control of Continuous Free Radical Polymerization Reactors. Ph.D. Thesis, Department of Chemical Engineering, University of Maryland, College Park, MD, 1991.

(29) Mohideen, M. J.; Perkins, J. D.; Pistikopoulos, E. N. Robust Stability Considerations in Optimal Design of Dynamic Systems under Uncertainty. *J. Process Control* **1997**, *7*, 371.

(30) Schweiger, C. A.; Floudas, C. A. Interaction of Design and Control: Optimization with Dynamic Models. In *Optimal Control: Theory, Algorithms and Applications*; Hager, W. W., Pardalos, P. M., Eds.; Kluwer Academic B. V.: Dordrecht, The Netherlands, 1997; pp 388−435.

(31) Bansal, V. Analysis Design and Control Optimization of Process System under Uncertainty. Ph.D. Thesis, Imperial College, University of London, London, U.K., 2000.

(32) Bansal, V.; Sakizlis, V.; Ross, R.; Perkins, J. D.; Pistikopoulos, E. N. New Algorithms for Mixed-Integer Dynamic Optimization. *Comput. Chem. Eng.* **2003**, *27*, 647.

(33) O'Driscoll, K. F.; Bevington, J. C. The Effect of Multifunctional Initiators on Molecular Weight in Free Radical Polymerization. *Eur. Polym. J.* **1985**, *21*, 1039.

(34) Choi, K. Y.; Lei, G. D. Modeling of Free-Radical Polymerization of Styrene by Bifunctional Initiators. *AIChE J.* **1987**, *33*, 2067.

(35) Kim, K. J.; Choi, K. Y. Modeling of Free Radical Polymerization of Styrene Catalyzed by Unsymmetrical Bifunctional Initiators. *Chem. Eng. Sci.* **1989**, *44*, 297.

(36) Villalobos, M. A.; Hamielec, A. E.; Wood, P. E. Kinetic Model for Short-Cycle Bulk Styrene Polymerization through Bifunctional Initiators. *J. Appl. Polym. Sci.* **1991**, *42*, 629.

(37) Yoon, W. J.; Choi, K. Y. Free-Radical Polymerization of Styrene with a Binary Mixture of Symmetrical Bifunctional Initiators. *J. Appl. Polym. Sci.* **1992**, *46*, 1353.

(38) Yoon, W. J.; Choi, K. Y. Kinetics of Free Radical Styrene Polymerization with the Symmetrical Bifunctional Initiator 2,5-Dimethyl-2,5-bis(2-ethyl hexanoyl peroxy) hexane. *Polymer* **1992**, *33*, 4582.

(39) González, I. M.; Meira, G. R.; Oliva, H. M. Synthesis of Polystyrene with Mixtures of Mono- and Bifunctional Initiators. *J. Appl. Polym. Sci.* **1996**, *59*, 1015.

(40) Dhib, R.; Gao, J.; Penlidis, A. Simulation of Free Radical Bulk/Solution Homopolymerization Using Mono- and Bifunctional Initiators. *Polym. React. Eng.* **2000**, *8*, 299.

(41) Cavin, L.; Rouge, A.; Meyer, Th.; Renken, A. Kinetic Modeling of Free Radical Polymerization of Styrene Initiated by the Bifunctional Initiator 2,5-Dimethyl-2,5-bis(2-ethyl hexanoyl peroxy) hexane. *Polymer* **2000**, *41*, 3925.

(42) Benbachir, M.; Benjelloun, D. Investigation of Free Radical Polymerization Using Diperoxyesters as Bifunctional Initiators. *Polymer* **2001**, *42*, 7727.

(43) Hui, A. W.; Hamielec, A. E. Thermal Polymerization of Styrene at High Conversions and Temperatures. An Experimental Study. *J. Appl. Polym. Sci.* **1972**, *16*, 749.

(44) Agarwal, S. S.; Kleinstreuer, C. Analysis of Styrene Polymerization in a Continuous Flow Tubular Reactor. *Chem. Eng. Sci.* **1986**, *41*, 3101.

(45) Prasad, V.; Schley, M.; Russo, L. P.; Bequette, B. W. Product Property and Production Rate Control of Styrene Polymerization. *J. Process Control* **2002**, *12*, 353.

(46) Perry, R. H.; Green, D. W. *Perry's Chemical Engineer's Handbook*; McGraw-Hill: New York, 1997.

(47) Russo, L. P.; Bequette, B. W. Operability of Chemical Reactors: Multiplicity Behaviour of a Jacketed Styrene Polymerization Reactor. *Chem. Eng. Sci.* **1998**, *53*, 27.

(48) Freitas Filho, I. P.; Biscaia, E. C., Jr.; Pinto, J. C. Steady-State Multiplicity in Continuous Bulk Polymerization Reactors—A General Approach. *Chem. Eng. Sci.* **1994**, *49*, 3745.

(49) Chylla, R. W.; Haase, D. R. Temperature Control of Semibatch Polymerization Reactors. *Comput. Chem. Eng.* **1993**, *17*, 257.

(50) Erdogan, S.; Alpbaz, M.; Karagoz, A. R. The Effect of Operational Conditions on the Performance of Batch Polymerization Reactor Control. *Chem. Eng. J.* **2002**, *86*, 259.

(51) Takamatsu, T.; Shioya, S.; Okada, Y. Molecular Weight Distribution Control in a Batch Polymerization Reactor. *Ind. Eng. Chem. Res.* **1988**, *27*, 93.

(52) Duran, M. A.; Grossman, I. E. An Outer-Approximation Algorithm for a Class of Mixed-Integer Nonlinear Programs. *Math. Program.* **1986**, *36*, 307.

(53) Kocis, G. R.; Grossmann, I. E. Relaxation Strategy for the Structural Optimization of Process Flowsheets. *Ind. Eng. Chem. Res.* **1987**, *26*, 1869.

(54) Viswanathan, J.; Grossmann, I. E. A Combined Penalty Function and Outer Approximation Method for MINLP Optimization. *Comput. Chem. Eng.* **1990**, *14*, 769.

Received for review January 21, 2004
Revised manuscript received May 26, 2004
Accepted May 28, 2004

IE040021S